Monthly Notices of the ROYAL ASTRONOMICAL SOCIETY

MNRAS **542,** 656–668 (2025) https://doi.org/10.1093/mnras/staf895
Advance Access publication 2025 June 2

Benchmark brown dwarfs – I. A blue M2 + T5 wide binary and a probable young [M4 + M4] + [T7 + T8] hierarchical quadruple

Z. H. Zhang (张曾华) [1,2]★ F. Navarete,[3] M. C. Gálvez-Ortiz,[4] H. R. A. Jones,[5] A. J. Burgasser [6] P. Cruz [4] F. Marocco [7] N. Lodieu,[8,9] Y. Shan,[10] B. Gauza [11] R. Raddi [12] M. R. Huang (黄缪锐),[1,2] R. L. Smart,[13] S. Baig [5] G. Cheng [5] and D. J. Pinfield[5]

[1]*School of Astronomy and Space Science, Nanjing University, 163 Xianlin Avenue, Nanjing 210023, China*
[2]*Key Laboratory of Modern Astronomy and Astrophysics, Nanjing University, Ministry of Education, Nanjing 210023, China*
[3]*Laboratório Nacional de Astrofísica (LNA/MCTI), Rua dos Estados Unidos, 154, 37504-364, Itajubá, MG, Brazil*
[4]*Centro de Astrobiología (CAB), CSIC-INTA, Camino Bajo del Castillo s/n, E-28692 Villanueva de la Cañada, Madrid, Spain*
[5]*Centre for Astrophysics Research, University of Hertfordshire, Hatfield, Hertfordshire AL10 9AB, UK*
[6]*Department of Astronomy & Astrophysics, University of California San Diego, La Jolla, CA 92093, USA*
[7]*IPAC, Caltech, Mail Code 100-22, 1200 E. California Boulevard, Pasadena, CA 91125, USA*
[8]*Instituto de Astrofísica de Canarias, E-38205 La Laguna, Tenerife, Spain*
[9]*Universidad de La Laguna, Dept. Astrofísica, E-38206 La Laguna, Tenerife, Spain*
[10]*Centre for Planetary Habitability, Department of Geosciences, University of Oslo, Sem Saelands vei 2b, 0315 Oslo, Norway*
[11]*Janusz Gil Institute of Astronomy, University of Zielona Góra, Lubuska 2, PL-65-265 Zielona Góra, Poland*
[12]*Universitat Politècnica de Catalunya, Departament de Física, c/ Esteve Terrades 5, E-08860 Castelldefels, Spain*
[13]*Istituto Nazionale di Astrofisica, Osservatorio Astronomico di Torino, Strada Osservatrio 20, I-10025 Pino Torinese, Italy*

Accepted 2025 May 30. Received 2025 May 30; in original form 2025 January 28

ABSTRACT

Benchmark brown dwarfs in wide binary systems are crucial for characterizing substellar objects and calibrating atmospheric and evolutionary models. However, brown dwarf benchmarks with subsolar metallicity, very cool temperatures, or suitability for dynamical mass measurements are rare, limiting our understanding across the full range of mass, age, and metallicity. We present the discovery of two new multiple systems containing T dwarf companions, identified through a targeted search using CatWISE2020 and *Gaia* catalogues. L 122–88 AB is a wide binary comprising a mildly metal-poor M2 dwarf and a T5 dwarf, separated by 215.6 arcsec at a distance of 33.106 ± 0.014 pc. Atmospheric model fitting to the near-infrared spectrum of L 122–88 A suggests a mildly metal-poor composition ([Fe/H] = −0.2). UPM J1040−3551 AB is a candidate hierarchical quadruple system at 25.283 ± 0.013 pc, consisting of a likely astrometric binary of two M4 dwarfs and a probable unresolved spectral binary of T7 and T8 dwarfs, separated by 65.48 arcsec from the primary. The Hα emission detected in UPM J1040−3551 A indicates an age range of 0.3–2.0 Gyr. This age estimate suggests that the T8 component has a mass between 9 and 28 Jupiter masses, potentially classifying it as a planetary-mass object. These systems augment the sample of benchmark brown dwarfs, particularly in the underexplored regime of cool temperature, providing valuable opportunities for refining our understanding of substellar objects.

Key words: planets and satellites: gaseous planets – binaries: general – brown dwarfs – stars: late-type – stars: low-mass.

1 INTRODUCTION

Brown dwarfs (BDs) are the most recently discovered major population on the Hertzsprung–Russell diagram. They mostly form like stars but lack sufficient mass to sustain steady hydrogen fusion. Consequently, BDs represent the low-mass tail of the initial mass function and are crucial for constraining it (Kirkpatrick et al. 2024). Bridging the gap between stars and planets, BDs share similar physical and atmospheric properties with gas giant planets (Hatzes & Rauer 2015), providing essential references for the characterization of exoplanets.

To address the scientific objectives outlined above, samples of well-characterized BDs are required. However, BDs are challenging to characterize due to their faintness, cool temperatures, and the mass–age degeneracy inherent in their evolution. Without steady hydrogen burning, BDs cool over time, altering their spectral features and types (e.g. fig. 8 of Burrows et al. 2001). Therefore, benchmark BD samples with known mass, age, metallicity, and luminosity, spanning a wide parameter space, are needed to test atmospheric and evolutionary models. This need is especially pressing in the era of ongoing and upcoming deep surveys such as *Euclid* (Laureijs et al. 2011), the *Roman Space Telescope* (Spergel et al. 2015), the Rubin Observatory (LSST Science Collaboration 2017), and the *Chinese Space Station Telescope* (*CSST*; Zhan 2011).

★ E-mail: zz@nju.edu.cn

BDs in nearby open clusters or moving groups with well-established ages serve as valuable age benchmarks [e.g. Teide 1 (Rebolo, Zapatero Osorio & Martín 1995) and Luhman 16 AB (Luhman 2013)]. However, these clusters and groups are predominantly young ($\lesssim$1 Gyr) and relatively distant ($\gtrsim$100 pc). In contrast, field BDs constitute the majority of the BD population, and span a broader range of ages and metallicities, with many residing in the solar neighbourhood. Yet, direct measurements of age or mass for individual field BDs remain elusive. None the less, BDs that are wide companions to well-characterized stars provide ideal benchmarks [e.g. Gliese 229 B (Nakajima et al. 1995) and ε Indi B (Scholz et al. 2003; McCaughrean et al. 2004; King et al. 2010)]. Binary systems are expected to have coeval formation, sharing common age, metallicity, and distance – parameters more readily determined for stars than for BDs. This characteristic makes such systems particularly valuable for BD studies.

The T dwarf spectral class was established to classify BDs cool enough to exhibit methane absorption in their near-infrared (NIR) spectra (Burgasser et al. 2002; Geballe et al. 2002). T dwarfs have effective temperatures ($T_{\rm eff}$) between ∼500 and 1300 K (Kirkpatrick et al. 2021). They constitute the majority of field BDs (e.g. Zhang et al. 2019). However, T dwarfs are relatively rare in observations due to their cool temperatures and low luminosities. About 900 spectroscopically confirmed T dwarfs are known to date, mostly within 30 pc of the Sun (see summary in Best et al. 2024). Two-thirds of known T dwarfs have spectral types of T5–T9, owing to the rapid evolution of BDs through the L/T transition (e.g. Best et al. 2021).

Currently, there are about 30 T dwarfs known with stellar companions (summarized in Best et al. 2024), with significant contributions from the *Wide-field Infrared Survey Explorer* (*WISE*; Wright et al. 2010). To expand the parameter space of benchmark T dwarfs and improve their characterization, we searched for late-type T dwarfs with wide stellar companions using the CatWISE2020 catalogue (Marocco et al. 2021) and the third data release (DR3) of *Gaia* (Gaia Collaboration 2023). In this paper, we present the discovery of a wide binary of mildly metal-poor M2 + T5 dwarfs and a probable young hierarchical quadruple system of [M4 + M4] + [T7 + T8] dwarfs. Section 2 describes the selection of wide binary candidates. Spectroscopic observation and characterization of these two systems are presented in Sections 3 and 4, respectively. A summary and conclusions are presented in Section 5.

2 SELECTION OF WIDE BINARIES

Wide binaries ($\gtrsim$100 au) exhibit negligible orbital motion over decadal time-scales due to their extremely long orbital periods ($\gtrsim$1 kyr). In the solar neighbourhood ($\lesssim$100 pc), the proper motions (PMs) of wide binary components significantly exceed their orbital motions, resulting in apparent common PM over decades. This characteristic makes common PM an effective method for identifying nearby wide binaries (e.g. Zhang 2019; Zhang et al. 2024).

T dwarfs emitting primarily in the infrared, only those in the solar neighbourhood, are detectable by large-scale infrared surveys. The CatWISE catalogue, providing mid-infrared photometry and PMs for nearby objects, serves as a powerful tool for identifying nearby T dwarf wide binaries.

We focused on late-type T dwarfs, which exhibit redder $W1-W2$ colour (equation 1) and suffer less contamination, e.g. from poorly measured background objects, than earlier types. Candidate selection from CatWISE employed the following criteria:

$$W1-W2>1.8, \tag{1}$$

$$W1\_{\rm snr}, W2\_{\rm snr}>5, \tag{2}$$

$${\rm PM}>100\ {\rm mas\ yr^{-1}}, \tag{3}$$

$${\rm PM_{RA}\_error}, {\rm PM_{Dec}\_error}<50\ {\rm mas\ yr^{-1}}, \tag{4}$$

$$|b|>10\ {\rm deg}, \tag{5}$$

$$nb=1, \tag{6}$$

$$ab\_{\rm flags}=00. \tag{7}$$

In our selection, we required signal-to-noise ratio (SNR) of better than 5.0 for $W1$ and $W2$ detections (equation 2). SNR of 5.0 corresponds to an error of ∼0.22 in $W1$ or $W2$ magnitudes. To mitigate contamination from background stars in the low-resolution (2.75 arcsec pixel^{-1}) unblurred coadds of the *WISE* images (unWISE; Lang 2014) used for CatWISE, we excluded the Galactic plane (equation 5).We select objects without identified artefacts in both $W1$- and $W2$-band unWISE images (equation 7) and with only one blend component used in the fit (equation 6). Approximately 9540 objects in CatWISE met these criteria (equations 1–7).

We then searched for wide companions of these objects in the *Gaia* Catalogue of Nearby Stars (GCNS; Gaia Collaboration 2021) using common PM. Our common PM pair criteria were

$$|{\rm PM_{RA1}}-{\rm PM_{RA2}}|, |{\rm PM_{Dec1}}-{\rm PM_{Dec2}}|<40\ {\rm mas\ yr^{-1}}, \tag{8}$$

$${\rm distance}<40\ {\rm pc}. \tag{9}$$

Given the relatively large PM errors in CatWISE, we required significant PM (equation 3) but relaxed the PM constraint in the GCNS cross-match (equation 8). The distance limit of 40 pc (equation 9) corresponds to the $W1$-band detection limit of CatWISE for late T dwarfs (e.g. table 6 of Zhang et al. 2019). We limited the binary separation to within 10 arcmin (corresponding to 24 000 au at 40 pc), beyond which the number of random contaminations arises, partially due to the large PM errors in CatWISE.

Our search yielded 15 candidate common PM pairs. After visual inspection using data from the Dark Energy Survey (Abbott et al. 2021) and the Dark Energy Spectroscopic Instrument (DESI) Legacy Imaging Surveys (Dey et al. 2019), we excluded seven pairs of which the faint component has poor unWISE images, has Dark Energy Camera (DECam) deep z-band non-detection ($z\gtrsim22.5$), or has no DECam observation and non-detection by other shallower surveys. The remaining eight T dwarf candidates, all with clear DECam z-band detections, comprise two newly identified wide binaries and six known wide systems [Gliese 570 A & D, K4V + T7.5 (Burgasser et al. 2000); G 204–39 AB, M3 + T6.5 (Faherty et al. 2010); SDSS J1416+13 AB, sdL7 + sdT7.5 (Burningham et al. 2010; Scholz 2010); HIP 73786 AB, sdM4 + sdT5.5 (Murray et al. 2011; Zhang et al. 2019); LHS 6176 AB, K8V + T8p (Burningham et al. 2013); and L 34–26 + COCONUTS-2b, M3V + T9 (Zhang et al. 2021)]. Fig. 1 shows the PMs of these common PM pairs.

The two new binaries, L 122–88 AB and UPM J1040−3551 AB, have been independently reported recently. Marocco et al. (2024) classified UCAC3 52–1038 B (i.e. L 122–88 B) as a T6 dwarf based on photometric colours, and classified UCAC3 52–1038 A (i.e. L 122–88 A) as an M2 dwarf based on its low-resolution

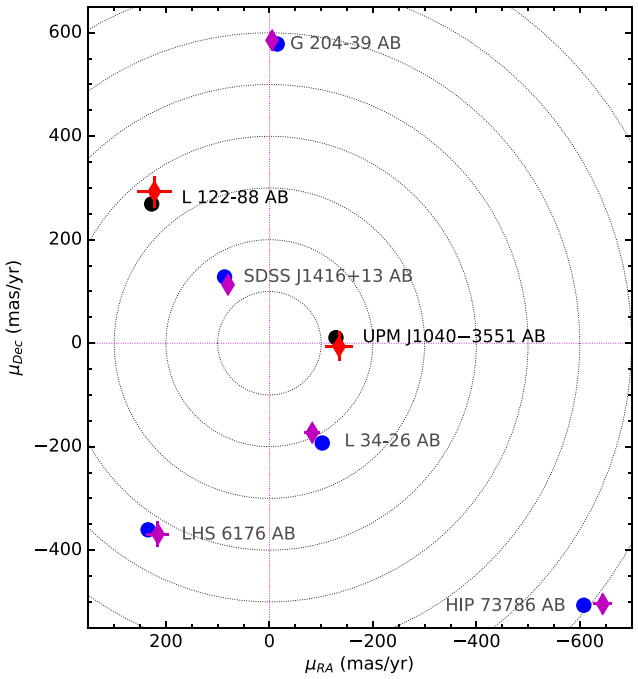

Figure 1. PMs of the newly discovered systems L 122–88 AB and UPM J1040−3551 AB, alongside the previously known systems: G 204–39 AB (M3 + T6.5), SDSS J1416+13 AB (sdL7 + sdT7.5), LHS 6176 AB (K8V + T8p), HIP 73786 AB (sdM4 + sdT5.5), and L 34–26 + COCONUTS-2b (M3V + T9) that were recovered in our search. Gliese 570 A & D (K4V + T7.5) are not shown because their PMs (2 arcsec yr^{-1}) are far exceeding the axis ranges. Black/blue dots represent *Gaia* PMs of primary stars (error bars are smaller than the symbol size), while red/magenta diamonds indicate CatWISE PMs of T dwarf secondaries.

optical spectrum observed on 2021 December 25. Rothermich et al. (2024) classified UPM J1040–3551 A as an M3.8 dwarf based on photometric colours, and classified UPM J1040–3551 B as T7 dwarf based on a low-resolution NIR spectrum observed on 2023 June 30. Fig. 2 shows the finding charts of these two new binaries. Their properties are listed in Table 1. The binary nature of these two newly identified pairs is corroborated by the concordance between the *Gaia* parallax-derived distances of the stellar components and the spectroscopically determined distances of their BD companions (Section 4.2).

L 122–88 AB and UPM J1040−3551 AB are located at distances of 33 and 25 pc, respectively. They were missed by earlier searches with *WISE* and AllWISE (Wright et al. 2010; Mainzer et al. 2011), possibly because T dwarf candidates within 20 pc were prioritized in those spectroscopic follow-up programmes, to achieve a more complete volume-limited sample (e.g. Kirkpatrick et al. 2011, 2021; Mace et al. 2013). Another seven known T dwarf binaries were selected as T dwarf candidates by equations (1)–(7), but were not recovered as wide binaries mainly because of large uncertainties of their CatWISE PMs. We recovered most of them by double the limits in equations (3) and (4), but no new binary T dwarf candidate was found.

3 SPECTROSCOPIC OBSERVATIONS

We conducted spectroscopic follow-up observations of L 122–88 AB and UPM J1040–3551 AB prior to their independent reporting. As spectra for L 122–88 B and UPM J1040−3551 A were not available in the literature, we continued our spectroscopic campaign to complete the analysis of these new binary systems. Table 2 summarizes the details of our observations.

3.1 SOAR/Goodman

L 122–88 A and UPM J1040–3551 A were observed using the Goodman High Throughput Spectrograph (Goodman; Clemens, Crain & Anderson 2004) at the Southern Astrophysical Research (SOAR) telescope in long-slit mode on 2023 December 29 (see Fig. 3). We used a 1 arcsec slit and the 400 lines mm^{-1} grism in M2 mode, providing wavelength coverage from 492 to 897 nm with a resolving power of ∼2000. Observations were conducted at airmass of 1.89 and seeing of 1.55 for L 122–88 A, and airmass of 1.04 and seeing of 1.45 for UPM J1040–3551 A.

Data reduction was performed using the Goodman High Throughput Spectrograph Pipeline[1] for basic CCD reduction, including bias subtraction, flat-field correction, and cosmic ray removal. Further spectroscopic processing utilized tasks from the NOAO package in IRAF, including wavelength calibration, spectral extraction, telluric correction, and flux calibration. HIP 45167 served as the telluric standard star for flux calibration.

3.2 SOAR/TripleSpec

UPM J1040−3551 B and L 122–88 B were observed with the TripleSpec4.1 NIR Imaging Spectrograph (TripleSpec; Schlawin et al. 2014) at SOAR. TripleSpec provides simultaneous spectral coverage from 940 to 2470 nm ($R \sim 3500$), spanning the entire $YJHK$ photometric range (see Fig. 4). UPM J1040−3551 B was observed on 2024 March 26 (seeing: 0.91 arcsec, airmass: 1.07), while L 122–88 B was observed on 2024 July 11 (seeing: 1.24 arcsec, airmass: 1.35). We adopted the default ABBA dither pattern with eight 225-s exposures for UPM J1040–3551 B and twenty 200-s exposures for L 122–88 B.

Data reduction employed a modified version of the IDL-based Spextool pipeline (Cushing, Vacca & Rayner 2004), adapted for SOAR. The process included flat-field correction, wavelength calibration using a CuHeAr arc lamp, removal of emission sky features by subtracting A and B exposures, and one-dimensional spectral extraction. Telluric correction and flux calibration were performed using observations of the standard star HIP 54311. The resulting NIR spectra exhibit peak SNRs of ∼10–15 at the centre of the YJH bands.

3.3 VLT/X-shooter

The X-shooter spectrograph (Vernet et al. 2011) at the Very Large Telescope (VLT) comprises three spectroscopic arms [UV-Blue (UVB), Visible (VIS), and NIR], each optimized for its spectral range (300–2500 nm). The optical to NIR spectrum of L 122–88 A was obtained using the X-shooter on 2024 June 16 (seeing: 1.5 arcsec, airmass: 1.8). Fig. 5 presents the combined, smoothed X-shooter spectrum of L 122–88 A.

L 122–88 B was observed with X-shooter on 2024 July 7 (seeing: 3.58 arcsec) and 2024 July 13 (seeing: 1.29 arcsec). Fig. 6 shows the X-shooter spectrum of L 122–88 B; noting that the optical spectrum is contaminated by a nearby galaxy, in fact, we note the presence of a non-zero continuum in the 400–800 nm spectral region in

[1] https://soardocs.readthedocs.io/projects/goodman-pipeline/

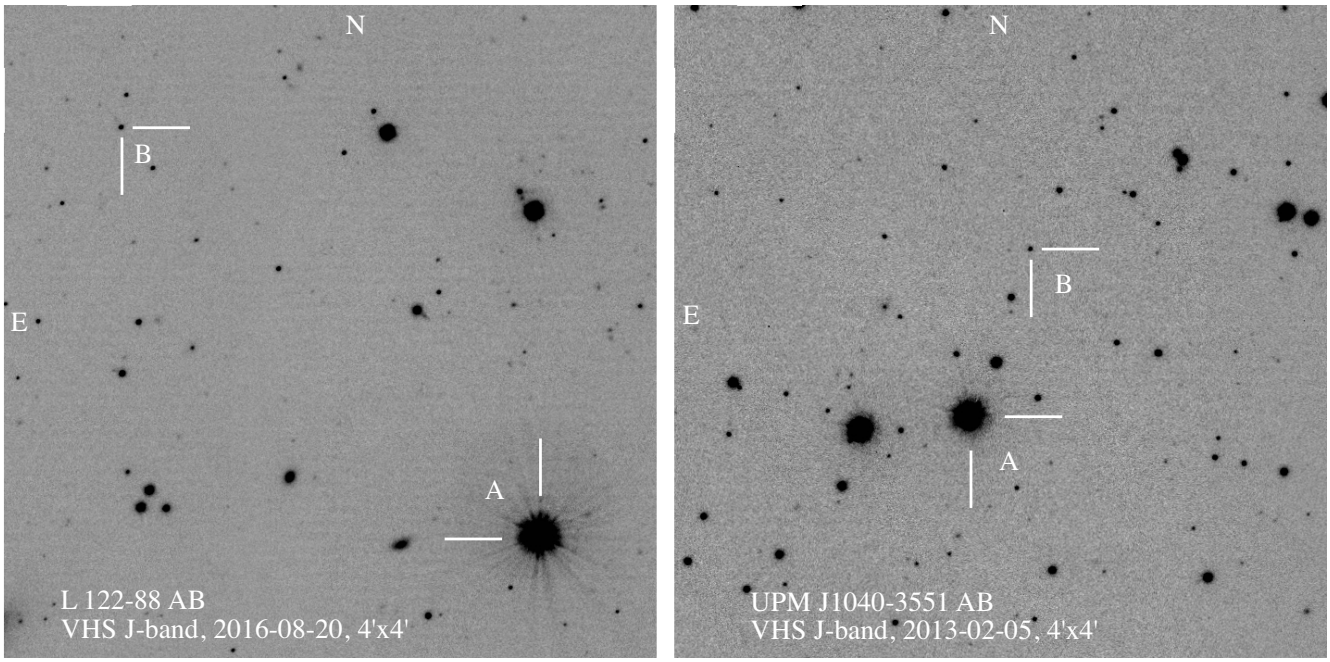

Figure 2. VISTA J-band images of the fields surrounding L 122–88 AB (left panel) and UPM J1040−3551 AB (right panel), which are indicated with white bars of 20 arcsec in length. Both images cover a 4 arcmin field of view, oriented with north up and east to the left. Observation dates are shown in yyyy-mm-dd format. L 122–88 AB is moving towards the north-east with a PM of 0.368 arcsec yr^{-1}, while UPM J1040−3551 AB is moving westwards with a PM of 0.135 arcsec yr^{-1} (see Fig. 1 for PM details).

which T dwarfs should barely have emitted any flux (e.g. Burgasser et al. 2003b). The nearby galaxy is faint in the J band (see Fig. 2) but brighter than L 122–88 B in the optical. With a PM of 0.368 arcsec yr^{-1} towards the north-east, L 122–88 B has moved to the top of the galaxy in 2024 when the X-shooter spectrum was taken. Meanwhile, the flux of the X-shooter spectrum beyond 2250 nm is poorly extracted/calibrated due to low SNR. These spectra were reduced using the European Southern Observatory Reflex pipeline (Freudling et al. 2013).

4 CHARACTERIZATION

4.1 M dwarf companions

The *Gaia* Renormalized Unit Weight Error (RUWE) values for L 122–88 A and UPM J1040−3551 A (1.32 and 1.47, respectively) suggest that these objects may potentially be unresolved binaries. However, their optical spectra appear consistent with normal M dwarfs (Fig. 3), indicating that if they are indeed binaries, each component likely possesses a similar spectral classification. Under such circumstances, given their identical distances, metallicity constraints derived from model fitting, whether applied to their composite spectra or to individual components, would yield consistent results. In this section, we first examine their spectra as single objects, then discuss their binarity in Section 4.1.4.

4.1.1 L 122–88 A

We compared the optical spectrum (Fig. 3) of L 122–88 A to those M0–M9 dwarf templates from Bochanski et al. (2007), and found that it closely matches an M2 dwarf template. However, it exhibits slightly weaker TiO absorption bands around 710 nm, which indicates a mildly metal-poor composition (e.g. Lépine, Rich & Shara 2007; Jao et al. 2008; Zhang 2019).

Analysis of data from the*Transiting Exoplanet Survey Satellite* (*TESS*; Ricker et al. 2015) using the TESSILATOR software (Binks & Günther 2024) reveals a rotation signal of 2.475 ± 0.013 d in sector 2 data. Applying gyrochronology to this rotation period using GPgyro (Lu et al. 2024) yields an age estimate of 0.029 ± 0.010 Gyr. However, there is no evidence for this signal in other *TESS* sectors (28, 29, 68, and 69). Examination of the *TESS* data sector 2 release notes[2] for TIC 271503151 (L 122–88 A) does not suggest any particular issue with the sector 2 observation, but for a $V = 13$ object we would expect the signal to be visible in other sectors for a reliable detection. Marocco et al. (2024) suggested a significantly older kinematic age of 2.5–9.9 Gyr for L 122–88 A.

4.1.2 UPM J1040−3551 A

We compared the optical spectrum (Fig. 3) of UPM J1040−3551 A to those M0–M9 dwarf templates from Bochanski et al. (2007), and found that it closely matches that of an M4 dwarf template. The presence of Hα emission in its spectrum indicates that it is an active M4 dwarf, which is also suggestive of a relatively young age. We measured the Hα equivalent width (Hα EW) of UPM J1040−3551 A to be between 2.33 and 3.78 Å. Applying the Hα activity–age correlation for M3–M6 dwarfs from Kiman et al. (2021) (their fig. 6), this Hα EW range corresponds to an estimated age of 0.3–2.0 Gyr. The *TESS* data for UPM J1040−3551 A show no indication of activity or any periodic signal.

[2]https://ntrs.nasa.gov/citations/20190001284

Table 1. Properties of L 122–88 AB and UPM J1040−3551 AB.

Primary	L 122–88 A	UPM J1040−3551 Aa/Ab	Ref.
CWISE	J003124.30−641354.9	J104055.33−355130.9	
Gaia DR3	4708465482876995712	5443160355149610368	(1)
α (2016)	$00^h31^m24^s.32$	$10^h40^m55^s.32$	(1)
δ (2016)	$-64°13'54''.8$	$-35^h51^m30^s.9$	(1)
Spectral type	M2	M4 + M4	(2)
Age (Gyr)	2.5–9.9	0.3–2.0	(3, 2)
RUWE	1.32	1.47	(1)
G	12.209	13.230	(1)
G_{BP}	13.346	14.863	(1)
G_{RP}	11.151	11.997	(1)
J (2MASS)	9.812 ± 0.026	10.302 ± 0.023	(4)
H (2MASS)	9.248 ± 0.023	9.676 ± 0.022	(4)
K (2MASS)	8.991 ± 0.019	9.446 ± 0.023	(4)
$W1$	8.868 ± 0.012	9.280 ± 0.012	(5)
$W2$	8.729 ± 0.007	9.087 ± 0.007	(5)
ϖ (mas)	30.206 ± 0.013	39.552 ± 0.020	(1)
Distance (pc)	33.106 ± 0.014	25.283 ± 0.013	(1)
μ_{RA} (mas yr^{-1})	227.556 ± 0.014	-128.580 ± 0.019	(1)
μ_{Dec} (mas yr^{-1})	269.121 ± 0.014	10.646 ± 0.018	(1)
V_{tan} (km s^{-1})	55.304 ± 0.023	15.462 ± 0.008	(1)
RV (km s^{-1})	15.63 ± 0.31	-0.09 ± 3.72	(1)
M_K	6.391 ± 0.020	7.432 ± 0.024	(2)
T_{eff} (K)	3618 ± 157	3244 ± 157	(6)
T_{eff} (K)	3500 ± 50	3200 ± 50	(2)
[Fe/H]	-0.2 ± 0.1	0.0 ± 0.1	(2)
Mass ($M_\odot$)	0.378 ± 0.020	$0.174 \pm 0.022/0.165 \pm 0.020$	(6, 2)
Companion B	L 122–88 B	UPM J1040−3551 Ba/Bb	
CWISE	J003147.79−641123.1	J104053.42−355029.7	
α (*WISE*)	$00^h31^m47^s.79$	$10^h40^m53^s.42$	(3)
δ (*WISE*)	$-64°11'23''.1$	$-35^h50^m29^s.7$	(3)
Mean MJD (d)	57265.87	57124.73	(3)
Spectral type	d/sdT5	T7 + T8	(2)
r (DECaPS)	25.149 ± 0.427	–	(7)
i (DECaPS)	23.824 ± 0.216	–	(7)
z (DECaPS)	21.107 ± 0.035	21.133	(7)
Y (DECaPS)	19.821 ± 0.046	–	(7)
J (VHS)	17.601 ± 0.015	17.393 ± 0.022	(8)
Ks (VHS)	18.417 ± 0.239	17.344 ± 0.128	(8)
$W1$	17.380 ± 0.055	16.773 ± 0.041	(5)
$W2$	15.351 ± 0.029	14.940 ± 0.025	(5)
Distance (pc)	45^{+21}_{-17}	$^a20^{+9}_{-8}$, $^b29^{+11}_{-14}$	(2)
μ_{RA} (mas yr^{-1})	222 ± 33	-135 ± 27	(5)
μ_{Dec} (mas yr^{-1})	293 ± 30	-6 ± 28	(5)
Mass ($M_\odot$)	0.05–0.067	0.011–0.033/0.009–0.027	(2)
Separation (arcsec)	215.6	65.48	(2)
Proj. sep. (au)	7138.4 ± 0.5	1655.6 ± 0.3	(2)
[c]Proj. sep. (r_J)	0.034	0.008	(2)
$-U$ (J)	5.6×10^{33}	1.3×10^{34}	(2)

Notes. References: (1) Gaia Collaboration (2023); (2) This paper; (3) Marocco et al. (2024); (4) Skrutskie et al. (2006); (5) Marocco et al. (2021); (6) Stassun et al. (2019); (7) Dey et al. (2019); and (8) McMahon et al. (2013).
[a]Average spectroscopic distance as a single T7 dwarf based on spectral type – absolute magnitudes in J, K, $W1$, and $W2$ bands (Zhang et al. 2019).
[b]Average spectroscopic distance as a T7 + T8 binary. The extracted apparent magnitude of the T7 companion is used in the calculation.
[c]Projected separation in Jacobi radius (r_J, see Section 4.3).

4.1.3 Atmospheric properties

The optical spectrum is more sensitive to T_{eff} of M (sub)dwarfs, while the NIR spectrum is more sensitive to [Fe/H]. Therefore, the full optical–NIR spectral profile of M subdwarfs can have better constraints of their T_{eff} and [Fe/H]. To derive the atmospheric parameters of L 122–88 A, we fitted its X-shooter spectrum (300–2500 nm) to BT-Settl models with 2600 K $\leq T_{eff} \leq$ 4500 K, $-1.0 \leq$ [Fe/H] ≤ 0.5, and $\log g = 5.0$ (Allard 2014). We used a typical $\log g = 5.0$ for M2–M4 dwarfs as $\log g$ has relatively small effect on their spectra compared to T_{eff} and [Fe/H]. We applied smoothing to

Table 2. Summary of the characteristics of the spectroscopic observations made with SOAR and VLT.

Name	SpT	UT date	Telescope	Instrument	Slit (arcsec)	Seeing (arcsec)	Airmass	Wavelength (nm)	Resolution ($\lambda/\delta\lambda$)	$T_{\rm int}$ (s)
UPM J1040–3551 A	M5	2023-12-29	SOAR	Goodman/400	1.0	1.45	1.04	492–897	2000	1 × 75
UPM J1040–3551 B	T7 + T8	2024-03-26	SOAR	TripleSpec	1.1	0.91	1.07	940–2470	3500	8 × 225
L 122–88 A	M2	2023-12-29	SOAR	Goodman/400	1.0	1.55	1.89	492–897	2000	1 × 75
—— " ——	— " —	2024-06-16	VLT	X-shooter/UVB	1.3	1.25	1.36	294–593	4000	2 × 64
—— " ——	— " —	—— " ——	—— " ——	X-shooter/VIS	—— " ——	—— " ——	— " —	526–1048	6700	2 × 93
—— " ——	— " —	—— " ——	—— " ——	X-shooter/NIR	—— " ——	—— " ——	— " —	983–2480	4300	4 × 50
L 122–88 B	d/sdT5	2024-07-11	SOAR	TripleSpec	1.1	1.24	1.35	940–2470	3500	20 × 200
—— " ——	— " —	2024-07-07	VLT	X-shooter/VIS	1.2	3.58	1.32	526–1048	6700	2 × 1474
—— " ——	— " —	—— " ——	—— " ——	X-shooter/NIR	—— " ——	—— " ——	— " —	983–2480	4300	10 × 300
—— " ——	— " —	2024-07-13	VLT	X-shooter/VIS	1.2	1.29	1.45	526–1048	6700	2 × 1474
—— " ——	— " —	—— " ——	—— " ——	X-shooter/NIR	—— " ——	—— " ——	— " —	983–2480	4300	10 × 300

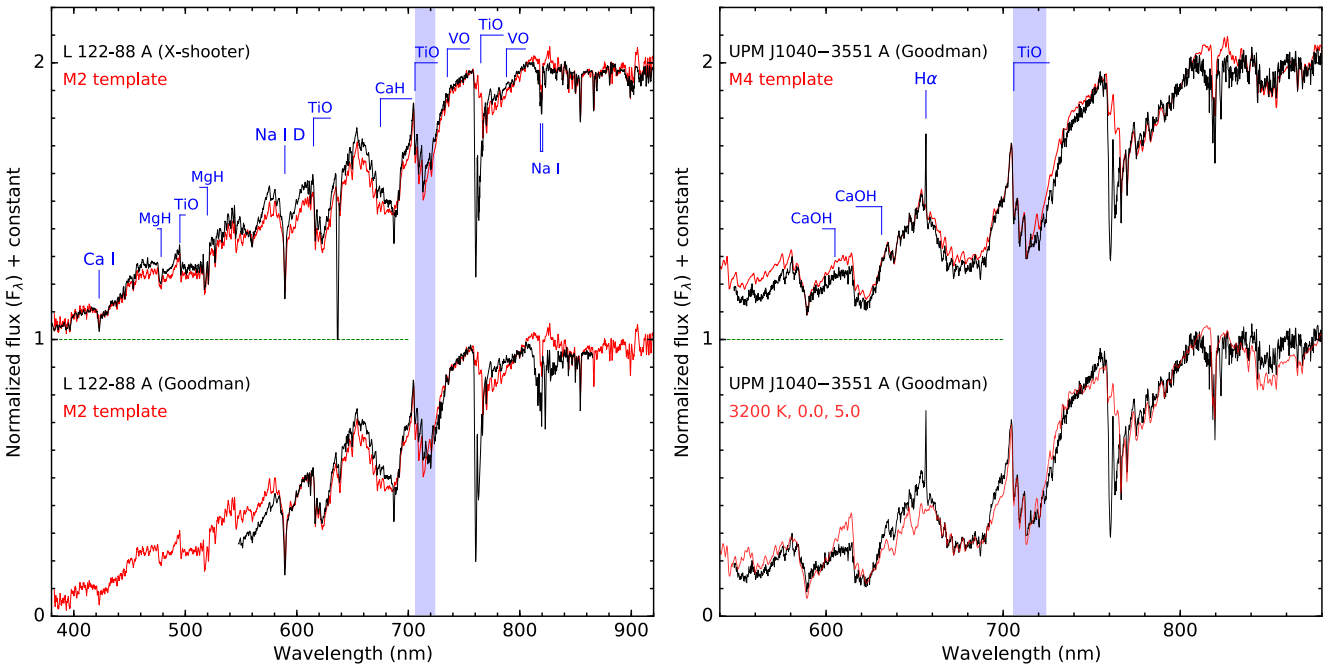

Figure 3. Optical spectra of L 122–88 A (left panel) and UPM J1040−3551 A (right panel) compared to M2 and M4 templates from Bochanski et al. (2007), respectively. The lower spectrum in the right panel shows the best-fitting BT-Settl model ($T_{\rm eff}$ = 3200 K, [Fe/H] = 0.0, and log g = 5.0) for UPM J1040−3551 A, degraded to a resolution of 0.5 nm. Note that telluric absorptions around 760 nm are not corrected for spectra of both primaries.

the X-shooter spectrum to enhance the SNR, though this degraded the resolving power to ∼1000. The BT-Settl model spectra were similarly degraded to match the resolution of the processed X-shooter spectrum.

The fitting procedure involved comparing the observed spectrum with a grid of models, varying $T_{\rm eff}$ in steps of 50 K and [Fe/H] in steps of 0.1 dex. We employed a least-squares method for the comparison. The best-fitting model for L 122–88 A yielded $T_{\rm eff} = 3500 \pm 50$ K, [Fe/H] $= -0.2 \pm 0.1$, and log $g = 5.0$ (Fig. 5), confirming its mildly metal-poor nature.

We applied a similar fitting procedure to the optical spectrum of UPM J1040−3551 A, using the same set of BT-Settl models. The best-fitting model for UPM J1040−3551 A resulted in $T_{\rm eff} = 3200$ K, [Fe/H] $= 0.0$, and log $g = 5.0$ (Fig. 3), indicating a solar metallicity for this object

4.1.4 UPM J1040–3551 A: a likely near equal-mass binary

Single stars are expected to have RUWE ≈ 1.0. Therefore, RUWE > 1.4 is usually used as an indicator of non-single object. Nearby M dwarfs and earlier type stars predominantly exhibit RUWE values of 1.2 ± 0.3 and 1.0 ± 0.2, respectively (Sozzetti 2023). The RUWE = 1.47 of UPM J1040–3551 A suggests it is likely an unresolved binary. For unresolved equal-mass binaries, the combined magnitude appears ∼0.75 mag brighter than each individual component, providing a method to test the binarity hypothesis.

UPM J1040–3551 A exhibits a typical $T_{\rm eff}$ (3200 ± 50 K) for M4 dwarfs (see fig. 4 of Zhang et al. 2018a). Notably, model spectral fitting would yield identical temperature estimates regardless of whether the object is a single star or an equal-mass binary. According to evolutionary models (Baraffe et al. 2015), a solar-metallicity star

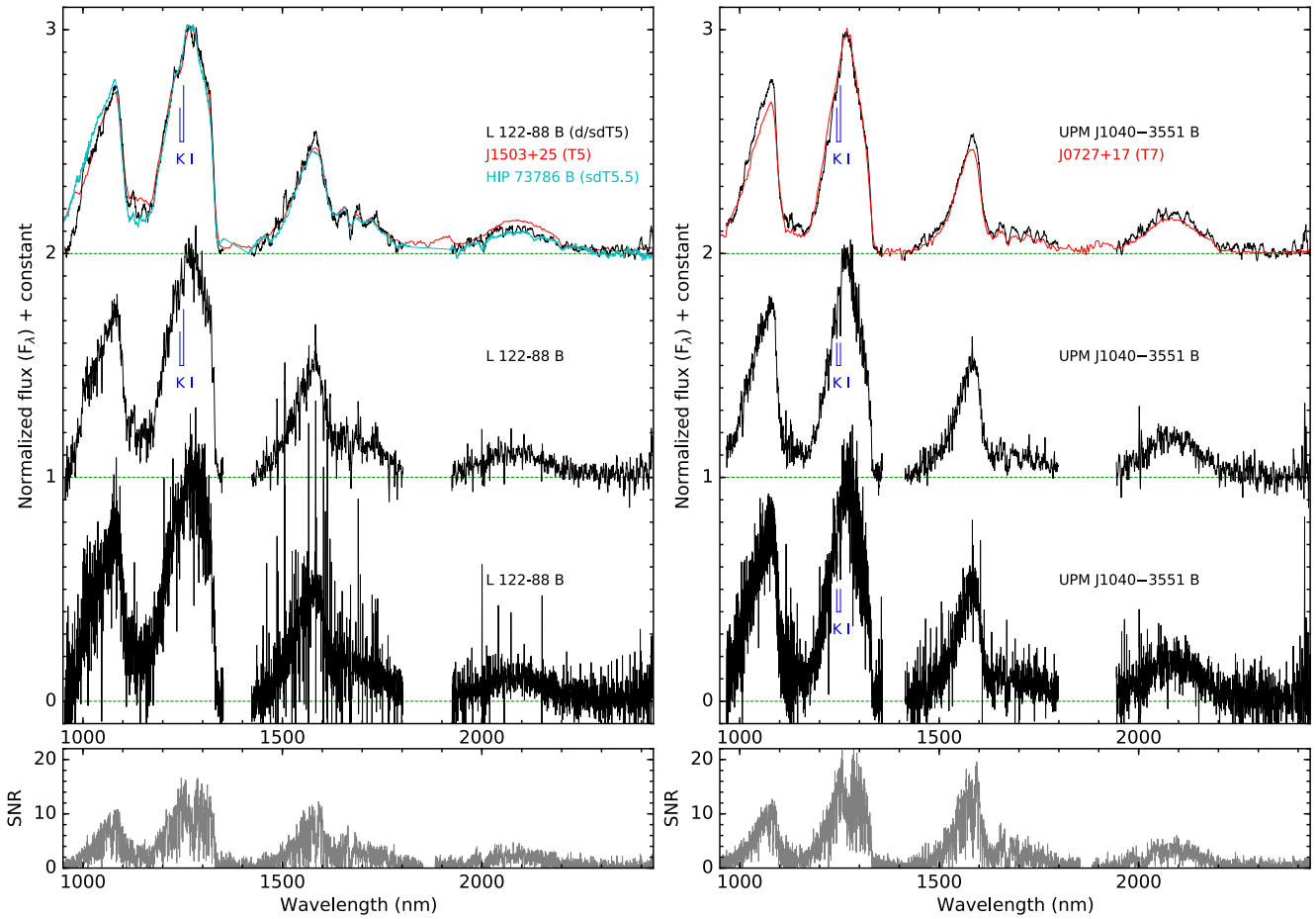

Figure 4. NIR spectra of L 122–88 B (left panel) and UPM J1040−3551 B (right panel) obtained with TripleSpec. The spectra are shown at original resolution (bottom) and smoothed by 11 pixels (middle) and 51 pixels (top). For comparison, we overplotted the spectra of the sdT5.5 subdwarf HIP 73786B (Zhang et al. 2019), the T5 dwarf standard 2MASS J15031961+2525196 (J1503+25; Burgasser et al. 2004), and the T7 dwarf standard 2MASS J0727182+171001 (J0727+17; Burgasser, Burrows & Kirkpatrick 2006).

with $T_{\rm eff}$ = 3200 K and age of 0.5-5 Gyr should have a mass of 0.174 $M_\odot$, radius of 0.195 $R_\odot$, and absolute magnitudes of M_J = 8.98, M_H = 8.39, and M_K = 8.13. The observed absolute magnitudes of UPM J1040–3551 A (M_J = 8.29, M_H = 7.66, and M_K = 7.432) are systematically brighter by 0.69, 0.73, and 0.70 mag, respectively, than predicted by models for its temperature (see Fig. 7). This consistent ∼0.7 mag excess strongly supports the classification of UPM J1040–3551 A as a near equal-mass binary system (UPM J1040–3551 Aab), with components Aa and Ab differing by only ∼0.1 mag ($\Delta T_{\rm eff}$ ∼ 25 K) and both can be classified as M4 dwarfs.

As a single star, UPM J1040–3551 A would have a mass of 0.235 ± 0.020 $M_\odot$ according to the mass-M_K correlation (Mann et al. 2019). A solar-metallicity star with this mass and age of 0.5-5 Gyr should have a $T_{\rm eff}$ = 3320 ± 40 K, significantly higher than the model spectral fitting result. With $T_{\rm eff}$ of 3200 K and 3175 K, UPM J1040–3551 Aa & Ab should have a mass around 0.174 ± 0.022 $M_\odot$ and 0.165 ± 0.020 $M_\odot$, respectively, according to evolutionary models (Baraffe et al. 2015).

For comparison, we also evaluated L 122-88 A by comparing its observed M_J, M_H, and M_K values to evolutionary model predictions for a solar-metallicity star with $T_{\rm eff}$ = 3500 K and age of 8 Gyr (see Fig. 7). The resulting magnitude differences of approximately 0.11 mag are insufficient to suggest binarity in this cas

4.2 T dwarf companions

Figure 4 presents the NIR spectra of L 122–88 B and UPM J1040−3551 B obtained with TripleSpec. These spectra have been smoothed to facilitate comparison with T dwarf standards. Our analysis of L 122–88 B primarily relies on its TripleSpec spectrum, which offers higher SNR compared to its X-shooter spectrum (Fig. 6).

4.2.1 L 122–88 B

The NIR spectrum of L 122–88 B (Figs 4 and 6) fits well to that of the T5 standard 2MASS J15031961+2525196 (J1503+25; Burgasser et al. 2003a, 2004), but exhibits suppressed K-band flux, which is a subsolar metallicity feature of BDs (Burgasser et al. 2002; Zhang et al. 2017a). It bears a strong resemblance to the sdT5.5 subdwarf benchmark HIP 73786 B (Murray et al. 2011; Zhang et al. 2019), which has a metallicity of $-0.30 \lesssim$ [Fe/H] $\lesssim -0.38$ inferred from its primary HIP 73786 A (Carollo et al. 2007; Soubiran et al. 2016; Arentsen et al. 2019). The slightly weaker K-band flux suppression in L 122–88 B compared to HIP 73786 B suggests a marginally higher metallicity, consistent with the metallicity derived from model fitting of L 122–88 A ([Fe/H] = 0.2 ± 0.1, Section 4.1). Consequently, we classify L 122–88 B as a mildly metal-poor T5 dwarf (d/sdT5).

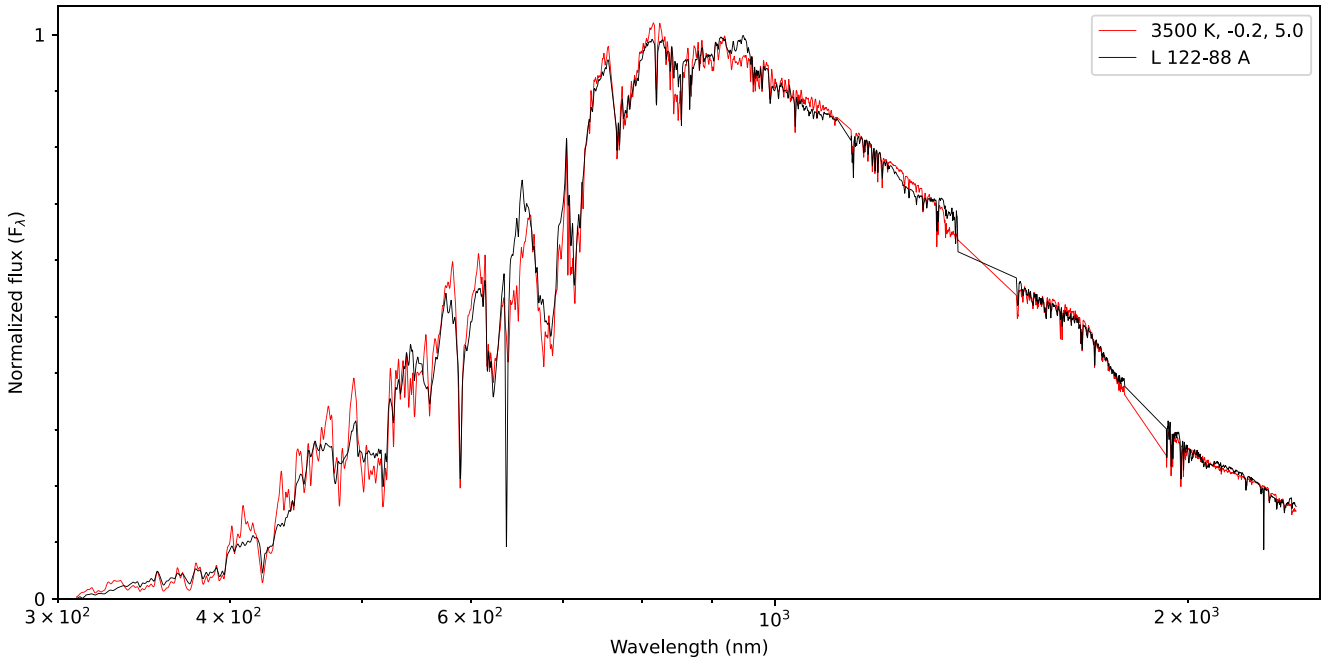

Figure 5. The X-shooter spectrum of L 122–88 A and its best-fitting BT-Settl model spectrum ($T_{\rm eff} = 3500$ K, [Fe/H] $= -0.2$, and $\log g = 5.0$).

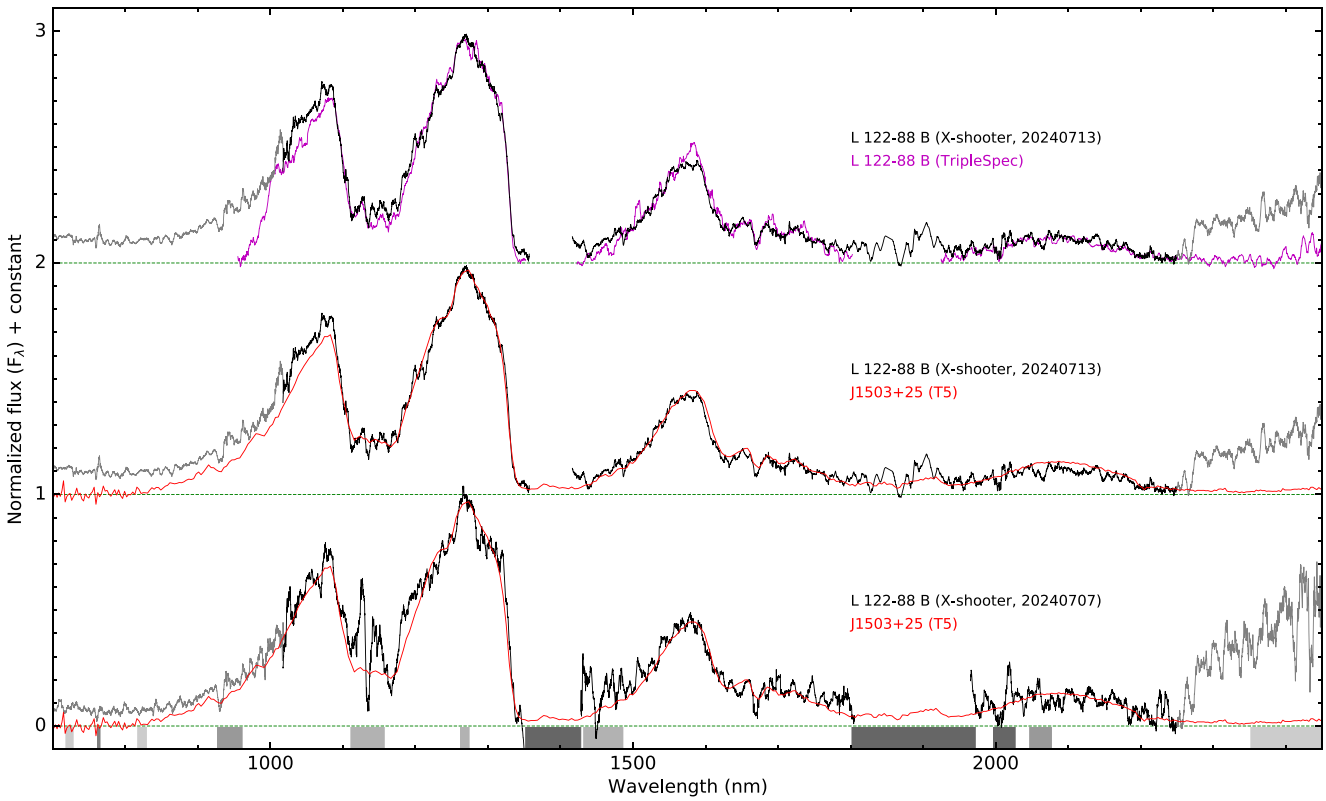

Figure 6. NIR spectra of L 122–88 B obtained with X-shooter on 2024 July 7 (bottom panel) and July 13 (middle panel). The spectra have been smoothed by 201 pixels in the VIS arm and 101 pixels in the NIR arm. The July 13 spectrum of L 122–88 B is compared to its TripleSpec spectrum at the top panel. The spectrum of the T5 dwarf standard 2MASS J15031961+2525196 (J1503+25; Burgasser et al. 2004) is overplotted for comparison. Grey stripes at the bottom indicate telluric regions, which have been corrected in both spectra.

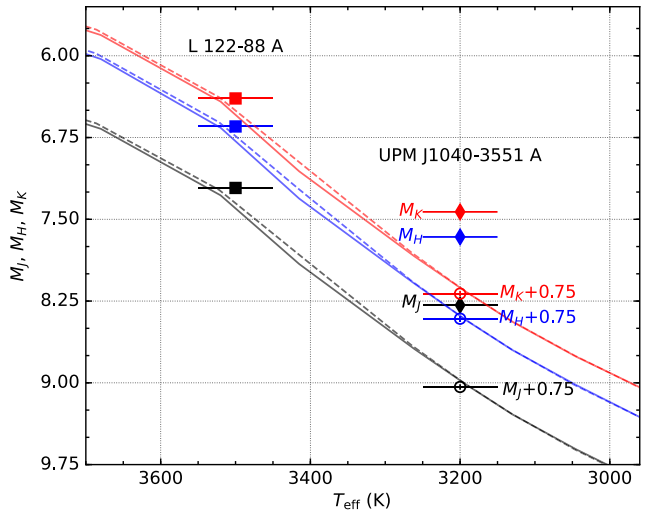

Figure 7 Observed M_J (black), M_H (blue), and M_K (red) absolute magnitudes of L 122-88 A (filled squires) and UPM J1040–3551 A (filled diamonds) compared to 1 Gyr (solid lines) and 8 Gyr (dashed lines) isochrones of solar-metallicity evolutionary models (Baraffe et al. 2015). Open circles indicate absolute magnitudes of an individual component of UPM J1040–3551 Aab, assumed as an equal-mass binary. Note, errors on absolute magnitudes are much smaller than symbol size.

HIP 73786 B exhibits a weak flux excess on the left-hand side of the Y-band peak (∼980–1080 nm), which is possibly caused by subsolar metallicity. This feature is also visible in spectra of other T subdwarfs with [Fe/H] $\lesssim -0.3$ and becomes more significant at lower metallicity (e.g. Pinfield et al. 2012; Burningham et al. 2014). The absence of the Y-band flux excess feature in L 122–88 B indicates a metallicity higher than that of T subdwarfs, which usually have [Fe/H] $\gtrsim -0.3$ (e.g. fig. 9 of Zhang et al. 2017b). This is still consistent with the metallicity derived from L 122–88 A.

To further investigate the mildly metal-poor nature of L 122–88 B, we compared its absolute magnitudes in the J, K, $W1$, and $W2$ bands, computed using the *Gaia* parallax of the primary, to those of known T dwarfs and subdwarfs (Fig. 8). L 122–88 B exhibits slightly fainter M_J, M_K, and M_{W1} compared to typical T5 dwarfs, while its M_{W2} remains similar. This pattern is consistent with the behaviour of T5.5-9 subdwarfs, which show fainter Y-, J-, H-, K-, and $W1$-band absolute magnitudes than their solar-metallicity counterparts, but indistinguishable $W2$-band absolute magnitudes (Zhang et al. 2019). Without considering its mildly metal-poor nature, L 122–88 B might be misclassified as a T6.5 ± 1 dwarf based on spectral type versus absolute magnitude correlations (Fig. 8). Indeed, Marocco et al. (2024) classified it as a T6 dwarf based on spectral type versus colour correlations from Kirkpatrick et al. (2021).

We also estimated the distance of L 122–88 B by the spectral type – absolute magnitude correlations (fig. 10 of Zhang et al. 2019). The average distance estimated from its J, K, $W1$, and $W2$ magnitudes is 45^{+21}_{-17} pc, which is consistent to the *Gaia* distance of L 122–88 A (33.106 ± 0.014) within the uncertainty. Of course, L 122–88 B exhibits an overestimated spectral distance due to its mildly metal-poor composition. This metallicity deficiency causes its actual absolute magnitudes to be fainter than the average values for T5 dwarfs used in the calculation.

4.2.2 *UPM J1040−3551 B: a probable unresolved binary*

The NIR spectrum of UPM J1040−3551 B closely resembles that of the T7 dwarf standard 2MASS J0727182+171001 (J0727+17; Burgasser et al. 2002, 2006). However, Fig. 4 reveals flux excesses in the Y, H, and K bands relative to the T7 standard when normalized at the J-band peak. When rescaling the spectrum of UPM J1040–3551 B to better align with the T7 standard across Y, H, and K bands, we observe a 13 per cent flux suppression in the J band, a phenomenon neither previously observed nor explained in any single BD.

Several features of evidence suggest that UPM J1040−3551 B is not a T subdwarf: (1) it exhibits K-band flux excess rather than the suppression typical of late-type T subdwarfs; (2) it has a relatively young age of 0.3–2.0 Gyr inferred from its primary (Section 4.1.2); and (3) it has solar metallicity as indicated by its primary's spectrum (Fig. 3). While the K-band flux excess could be attributed to its young age (e.g. Burningham et al. 2011), this explanation fails to account for the observed Y- and H-band flux excesses.

Unresolved binary BDs may show unusual spectral features and colours, and flux excesses if they have been treated as single objects (Burgasser et al. 2010; Zhang et al. 2010, 2018b; Marocco et al. 2015; Kirkpatrick et al. 2021). Fig. 8 demonstrates that UPM J1040−3551 B has significantly brighter J-, K-, and $W1$-band absolute magnitudes than typical T7 dwarfs. Such overluminosity in field ultracool dwarfs often indicates the presence of an unresolved companion.

To test this hypothesis, we conducted a binary spectral fitting analysis using single spectral templates in the Spex Prism Library Analysis Toolkit (SPLAT; Burgasser & Splat Development Team 2017). We selected 131 T4–T9 dwarfs with low-resolution ($\lambda/\Delta\lambda \approx$ 150) NIR spectra previously obtained with the Spectral cross-disperser (SpeX) spectrograph (Rayner et al. 2003) on the 3 m NASA Infrared Telescope Facility. These templates exclude known or suspected binaries and spectra with very low S/N $\lesssim$ 15. Spectra were interpolated and resampled on to a common wavelength scale spanning 0.95–2.5 μm at a constant resolution $\lambda/\Delta\lambda = 200$, classified by comparison to NIR spectral standards (Burgasser et al. 2006), and then flux-calibrated using the Kirkpatrick et al. (2021) absolute MKO J-band magnitude/spectral type relation. We then co-added pairs of spectra to create 6715 unique binary templates. We compared both single and binary templates to the equivalently interpolated SOAR spectrum of J1040−3551 B following procedures described in Burgasser et al. (2010), masking out regions of strong telluric absorption between 1.35–1.42 μm and 1.80–1.95 μm. Fig. 9 compares the best-fitting single template from this sample, the T7 dwarf WISE J004024.88+090054.8 (J0040+0900; Mace et al. 2013) to the best-fitting binary template composed of J0040+0900 and the T8 dwarf ULAS J102940.52+093514.6 (J1029+0935; Burningham et al. 2013; Thompson et al. 2013). The latter is a superior fit, notably providing a better reproduction of the Y-, H-, and K-band peaks. The difference in reduced χ^2 between the single fit (10.6) and the binary fit (7.6) implies a 2 per cent likelihood of equivalence based on the F-test statistic. However, we caution that other physical parameters, such as youth/low surface gravity, could also explain the modest deviations in the single template fit and may not be fully accounted for in the existing SPLAT template sample. The spectral fitting therefore provides supporting but not conclusive evidence of unresolved multiplicity.

To further investigate this binary hypothesis, we decomposed the absolute magnitudes of UPM J1040−3551 B into T7 and T8 components. Using the spectral type versus absolute magnitude

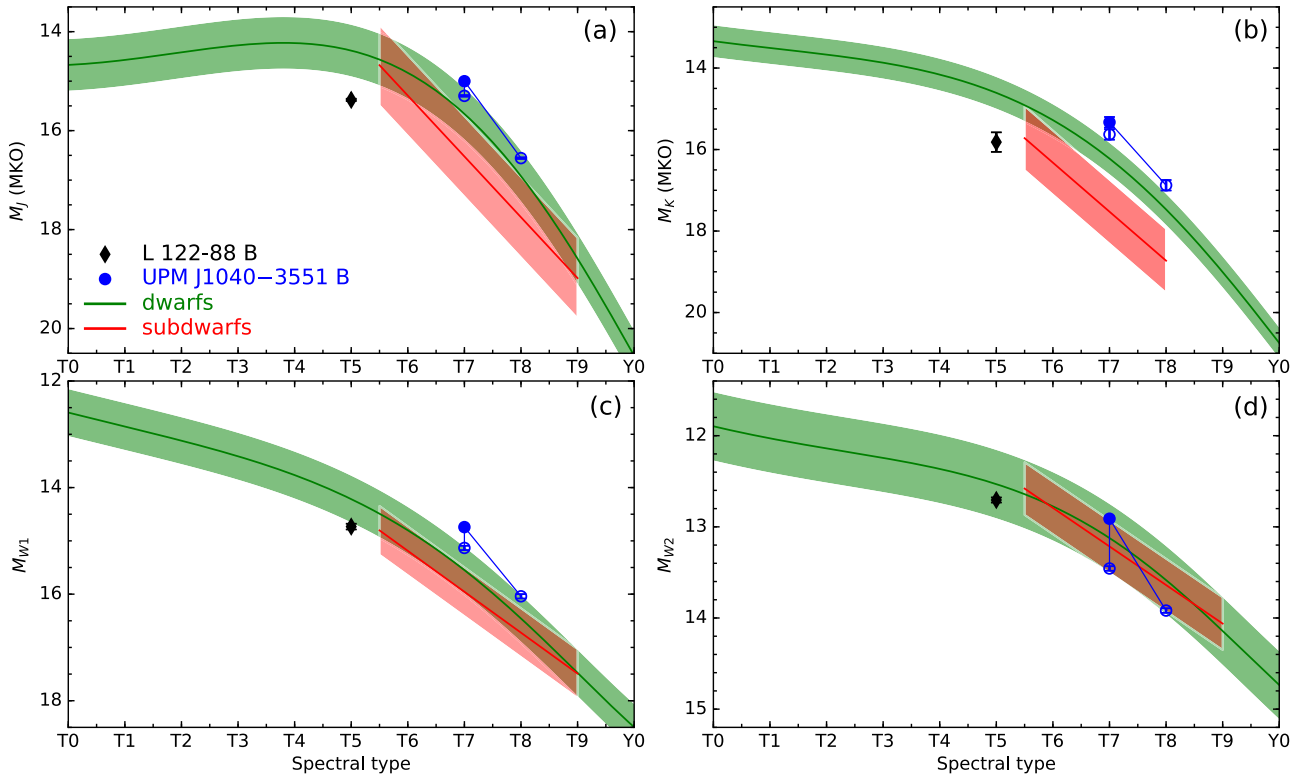

Figure 8. Absolute magnitudes (M_J, M_K, M_{W1}, and M_{W2}) of L 122–88 B (black diamond) and UPM J1040−3551 B (blue circle) plotted against spectral type. Long curved green and short straight red lines show the spectral type versus absolute magnitude correlations for dwarfs and subdwarfs, respectively, from fig. 10 of Zhang et al. (2019). The green shaded areas indicate the rms of these fits. Blue open circles represent the decomposed absolute magnitudes of UPM J1040−3551 Ba & Bb, obtained by splitting the magnitudes of UPM J1040−3551 B based on the average differences between T7 and T8 dwarfs.

correlations for L and T dwarfs (Fig. 8), we derived M_J, M_K, M_{W1}, and M_{W2} differences between T7 and T8 dwarfs of 1.258, 1.248, 0.907, and 0.462 mag, respectively. The decomposed M_J, M_K, and M_{W1} values demonstrate improved alignment with these correlations, though they remain slightly brighter than average – contrary to the dimmer characteristics of late T subdwarfs. UPM J1040−3551 B appears underluminous as an unresolved binary only in the $W2$ band, which may be attributed to its young age. For instance, the young T5.5 dwarf SDSSp J111010.01+011613.1 (Geballe et al. 2002) is relatively faint in the $W2$ band, with a $W1 - W2$ colour 0.34 mag bluer than the average for field T5.5 dwarfs (fig. 8i of Zhang et al. 2019).

The independent spectroscopic distance of UPM J1040−3551 B as a single T7 dwarf is 20^{+9}_{-8} pc, which is 21 per cent shorter than the *Gaia* distance of the M4 primary (25.283 ± 0.013 pc). We also decomposed the J-, K-, $W1$-, and $W2$-band apparent magnitudes of UPM J1040−3551 B as T7 + T8 close binary. The average spectroscopic distance of UPM J1040−3551 Ba as a T7 dwarf is 21^{+10}_{-8} pc, which is 17 per cent smaller than its UPM J1040−3551 A but consistent within the uncertainty. The spectral distance of UPM J1040−3551 B is underestimated due to its young age, which allows it to have brighter absolute magnitudes than the average values for T7 dwarfs used in the calculation.

Both the spectral fitting and the decomposition of absolute magnitudes strongly suggest that UPM J1040−3551 B is likely an unresolved T7 + T8 binary (UPM J1040−3551 Ba & Bb). UPM J1040−3551 AabBab is the first known quadruple system comprising a close binary of T dwarfs in a wide orbit around a close binary of stars. It is the third identified system featuring a close binary of T dwarfs with wide stellar companion, following ε Indi ABab (Scholz et al. 2003; McCaughrean et al. 2004; King et al. 2010) and Gliese 229 ABab (Xuan et al. 2024).

UPM J1040−3551 B is detected but not resolved in the Visible and Infrared Survey Telescope for Astronomy (VISTA) Hemisphere Survey (VHS; McMahon et al. 2013) and the Dark Energy Camera Legacy Survey (DECaLS; Dey et al. 2019). The VHS and DECaLS images have pixel sizes of 0.34 and 0.26 arcsec, respectively. This allows us to place upper limits on the orbital semimajor axis ($\lesssim$10 au) and period ($\lesssim$160 yr) of the system. At a distance of 25 pc, the components can potentially be resolved at 1.15 μm by the Near-Infrared Camera of the *JWST*, provided the orbital period exceeds six years.

4.3 Binary properties

To estimate the masses of the T dwarf companions, we employed the evolutionary tracks of $T_{\rm eff}$ from the Sonora-Bobcat models (Marley et al. 2021), using their estimated ages and the average $T_{\rm eff}$ of T dwarfs with corresponding spectral types. As illustrated in Fig. 10, L 122–88 B has an estimated mass of 0.05–0.067 M⊙ for an age of 2.5–9.9 Gyr, while UPM J1040−3551 Ba and Bb have estimated masses of 0.012–0.04 M⊙ and 0.007–0.02 M⊙, respectively, for an age of 0.3–2.0 Gyr. Using the derived distances, projected separations, and masses of all components, we calculated the binding energies of L 122–88 AB and UPM J1040−3551 AabBab to be 5.6×10^{33} and 1.3×10^{34} J, respectively.

To assess the stability of these wide binary systems, we considered the Jacobi (or tidal) radius (r_J), which represents the maximum

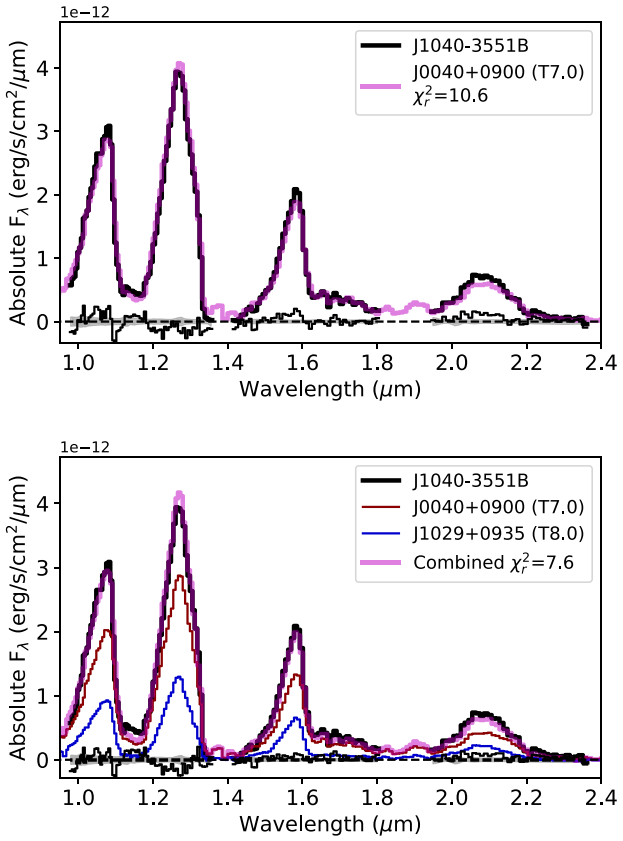

Figure 9. SOAR spectrum of UPM J1040−3551 B (black lines) scaled to absolute fluxes compared to best-fitting single (top panel) and binary templates (bottom panel; magenta lines) constructed from SpeX/prism spectra. In the bottom panel, we display also the relative scaling of the spectral components of the best-fitting binary, the T7 J0040+0900 (red line) and T8 J1029+0935 (blue line). Both panels compare the difference spectrum (black line centred at zero) to the uncertainty spectrum (grey band), and the reduced χ^2 is listed for each fit.

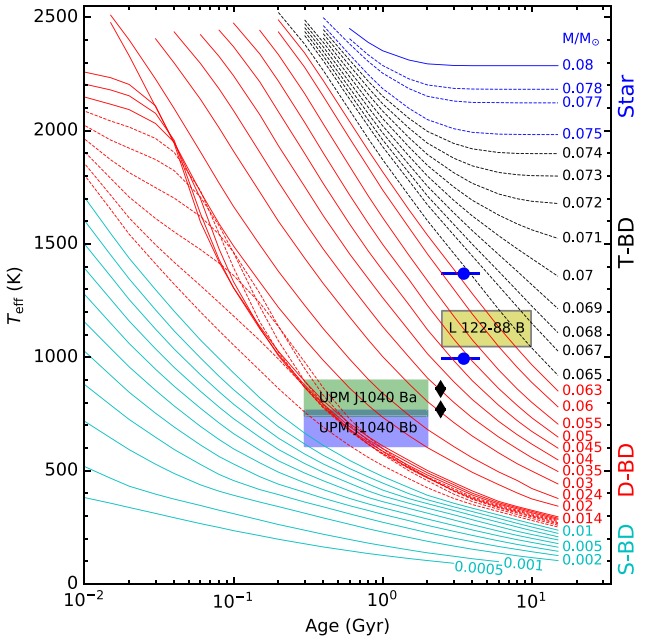

Figure 10. Evolutionary tracks of $T_{\rm eff}$ from the Sonora-Bobcat models (Marley et al. 2021) for objects with masses of 0.0005–0.08 $M_\odot$ and solar metallicity, spanning 0.02–15 Gyr. Tracks are colour-coded from top to bottom: blue for stars, black for transitional BDs (T-BDs; Zhang et al. 2018a), red for degenerate BDs (D-BDs; Zhang et al. 2019), and cyan for sub-BDs (S-BDs). Yellow, green, and blue shaded boxes indicate the estimated locations of L 122-88 B and UPM J1040−3551 Ba & Bb, respectively. For comparison, ε Indi BaBb (blue circles) and Gliese 229 BaBb (black diamonds) are also plotted. Note that stars with masses of 0.075–0.078 $M_\odot$ (blue dashed lines) keep reducing their $T_{\rm eff}$ and radii slowly until 8–10 Gyr according to the Sonora-Bobcat models. D-BDs with masses between 0.01 and 0.014 $M_\odot$ (red dashed lines) fuse partial of their deuterium and form a lithium burning transition zone (see fig. 5 of Zhang et al. 2019).

separation for stable wide binary systems. The r_J delineates the boundary beyond which the tidal field dominates over the gravitational attraction between the binary components. For wide binaries in the solar neighbourhood, r_J can be calculated using equation (43) from Jiang & Tremaine (2010).

We found that L 122–88 AB and UPM J1040−3551 AabBab have r_J values of ∼1.02 and ∼0.97 pc, respectively. Their projected separations correspond to 0.034 r_J and 0.008 r_J, respectively, which are far smaller than their respective r_J values. This analysis strongly suggests that both systems are gravitationally stable. The spectroscopic distances of L 122–88 B and UPM J1040−3551 B are also consistent to *Gaia* parallax distances of their primaries (see Table 1).

5 SUMMARY AND CONCLUSIONS

We have conducted a search for late T dwarf wide binaries using CatWISE and *Gaia* DR3, resulting in the discovery of a wide binary and a probable hierarchical quadruple system. Both systems are confirmed to be gravitationally bound and stable based on their tidal radii. Optical and NIR spectroscopic follow-up observations were performed for all companions, enabling spectral classification and characterization.

The first system, L 122–88 AB, exhibits spectral features indicative of mildly metal-poor composition, including a weaker 710 nm TiO absorption band in L 122–88 A and suppressed *K*-band flux in L 122–88 B. The best-fitting BT-Settl model to the 0.3–2.5 μm spectrum of L 122–88 A yields $T_{\rm eff}$ = 3500 K, [Fe/H] = −0.2, and log g = 5.0. We classify L 122–88 AB as a mildly metal-poor M2 + T5 wide binary.

The second system, UPM J1040−3551 AB, is likely a hierarchical quadruple system consisting of a T7 + T8 spectral binary and an M4 + M4 astrometric binary at a distance of 25 pc from the Sun. Both the RUWE (1.47) of UPM J1040–3551 A and its excess luminosity (0.7 mag brighter than model predications of its $T_{\rm eff}$) suggest it is an unresolved M4 + M4 binary. While UPM J1040−3551 Ba/Bb are unresolved in survey images, their NIR spectrum is best fitted by a combined T7 + T8 template, explaining the observed excess luminosity. UPM J1040–3551 AabBab is the first known quadruple system with a close binary of T dwarfs. Based on the Hα emission of the M4 primary, we estimate the system age to be 0.3–2 Gyr. At this relatively young age, the T8 component UPM J1040−3551 Bb has a mass between 9 and 28 Jupiter masses and potentially is a planetary-mass object.

These newly discovered systems, L 122–88 AB and UPM J1040−3551 AB, augment the sample of benchmark BDs, particularly in the less-explored regimes of cool temperature. UPM J1040−3551 B potentially is a good target for dynamical mass measurement with high-resolution imaging. They present valuable

opportunities for refining atmospheric and evolutionary models, thereby enhancing our understanding of substellar objects approaching the planetary-mass limit. Furthermore, these systems may provide crucial insights into bridging the gap between BDs and giant exoplanets, contributing to a more comprehensive understanding of the low-mass end of the stellar–substellar–planetary continuum.

ACKNOWLEDGEMENTS

This study is based on observations obtained at the SOAR telescope, which is a joint project of the Ministério da Ciência, Tecnologia e Inovações (MCTI/LNA) do Brasil, the US National Science Foundation's NOIRLab, the University of North Carolina at Chapel Hill (UNC), and Michigan State University (MSU). This study is based on observations collected at the European Southern Observatory under ESO programme 113.26V7.001.

This work has made use of data from the European Space Agency (ESA) mission *Gaia* (https://www.cosmos.esa.int/gaia), processed by the *Gaia* Data Processing and Analysis Consortium (DPAC; https://www.cosmos.esa.int/web/gaia/dpac/consortium). Funding for the DPAC has been provided by national institutions, in particular the institutions participating in the *Gaia* Multilateral Agreement. This publication makes use of data products from the *WISE*, which is a joint project of the University of California, Los Angeles, and the Jet Propulsion Laboratory/California Institute of Technology, funded by the National Aeronautics and Space Administration. SPLAT is a collaborative project of research students in the UCSD Cool Star Lab, aimed at developing research through the building of spectral analysis tools. Contributors to SPLAT have included Christian Aganze, Jessica Birky, Daniella Bardalez Gagliuffi, Adam Burgasser (PI), Caleb Choban, Andrew Davis, Ivanna Escala, Joshua Hazlett, Carolina Herrara Hernandez, Elizabeth Moreno Hilario, Aishwarya Iyer, Yuhui Jin, Mike Lopez, Dorsa Majidi, Diego Octavio Talavera Maya, Alex Mendez, Gretel Mercado, Niana Mohammed, Johnny Parra, Maitrayee Sahi, Adrian Suarez, Melisa Tallis, Tomoki Tamiya, Chris Theissen, and Russell van Linge.

ZHZ acknowledges the supports from the Jiangsu Province fundamental research programme (BK20211143), the Program for Innovative Talents and Entrepreneur in Jiangsu (JSSCTD202139), and the science research grants from the China Manned Space Project with no. CMS-CSST-2021-A08. The work of FN was supported by NOIRLab, which is managed by the Association of Universities for Research in Astronomy (AURA) under a cooperative agreement with the National Science Foundation. MCG-O acknowledges financial support from the Agencia Estatal de Investigación (AEI/10.13039/501100011033) of the Ministerio de Ciencia e Innovación and the ERDF 'A way of making Europe' through project PID2022-137241NB-C42. NL acknowledges support from the Agencia Estatal de Investigación del Ministerio de Ciencia e Innovación (AEI-MCINN) under grant PID2022-137241NB-C41. BG acknowledges support from the Polish National Science Center (NCN) under SONATA grant no. 2021/43/D/ST9/0194. PC acknowledges financial support from the Spanish Virtual Observatory project funded by the Spanish Ministry of Science and Innovation/State Agency of Research MCIN/AEI/10.13039/501100011033 through grant PID2020-112949GB-I00. The authors would like to thank the anonymous reviewer for his/her valuable comments.

DATA AVAILABILITY

The data underlying this article are available in the article and in its online supplementary material.

REFERENCES

Abbott T. M. C. et al., 2021, ApJS, 255, 20
Allard F., 2014, in Booth M., Matthews B. C., Graham J. R., eds, Proc. IAU Symp. 299, Exploring the Formation and Evolution of Planetary Systems. Cambridge Univ. Press, Cambridge, p. 271
Arentsen A. et al., 2019, A&A, 627, A138
Baraffe I., Homeier D., Allard F., Chabrier G., 2015. A&A, 577, A42
Best W. M. J., Dupuy T. J., Liu M. C., Sanghi A., Siverd R. J., Zhang Z., 2024, The UltracoolSheet: Photometry, Astrometry, Spectroscopy, and Multiplicity for 4000+ Ultracool Dwarfs and Imaged Exoplanets (2.0.0) [Data set]. Zenodo, https://doi.org/10.5281/zenodo.10573247
Best W. M. J., Liu M. C., Magnier E. A., Dupuy T. J., 2021, AJ, 161, 42
Binks A. S., Günther H. M., 2024, MNRAS, 533, 2162
Bochanski J. J., West A. A., Hawley S. L., Covey K. R., 2007, AJ, 133, 531
Burgasser A. J. et al., 2000, ApJ, 531, L57
Burgasser A. J. et al., 2002, ApJ, 564, 421
Burgasser A. J., Burrows A., Kirkpatrick J. D., 2006, ApJ, 639, 1095
Burgasser A. J., Cruz K. L., Cushing M., Gelino C. R., Looper D. L., Faherty J. K., Kirkpatrick J. D., Reid I. N., 2010, ApJ, 710, 1142
Burgasser A. J., Kirkpatrick J. D., Liebert J., Burrows A., 2003b, ApJ, 594, 510
Burgasser A. J., Kirkpatrick J. D., McElwain M. W., Cutri R. M., Burgasser A. J., Skrutskie M. F., 2003a, AJ, 125, 850
Burgasser A. J., McElwain M. W., Kirkpatrick J. D., Cruz K. L., Tinney C. G., Reid I. N., 2004, AJ, 127, 2856
Burgasser A. J., Splat Development Team, 2017, in Astronomical Society of India Conference Series. p. 7, preprint (arXiv:1707.00062)
Burningham B. et al., 2010, MNRAS, 404, 1952
Burningham B. et al., 2011, MNRAS, 414, 3590
Burningham B. et al., 2013, MNRAS, 433, 457
Burningham B., Smith L., Cardoso C. V., Lucas P. W., Burgasser A. J., Jones H. R. A., Smart R. L., 2014, MNRAS, 440, 359
Burrows A., Hubbard W. B., Lunine J. I., Liebert J., 2001, Rev. Mod. Phys., 73, 719
Carollo D. et al., 2007, Nature, 450, 1020
Clemens J. C., Crain J. A., Anderson R., 2004, in Moorwood A. F. M., Iye M., eds, Proc. SPIE Conf. Ser. Vol. 5492, Ground-based Instrumentation for Astronomy. SPIE, Bellingham, p. 331
Cushing M. C., Vacca W. D., Rayner J. T., 2004, PASP, 116, 362
Dey A. et al., 2019, AJ, 157, 168
Faherty J. K., Burgasser A. J., West A. A., Bochanski J. J., Cruz K. L., Shara M. M., Walter F. M., 2010, AJ, 139, 176
Freudling W., Romaniello M., Bramich D. M., Ballester P., Forchi V., García-Dabló C. E., Moehler S., Neeser M. J., 2013, A&A, 559, A96
Gaia Collaboration, 2021, A&A, 649, A6
Gaia Collaboration, 2023, A&A, 674, A1
Geballe T. R. et al., 2002, ApJ, 564, 466
Hatzes A. P., Rauer H., 2015, ApJ, 810, L25
Jao W.-C., Henry T. J., Beaulieu T. D., Subasavage J. P., 2008, AJ, 136, 840
Jiang Y.-F., Tremaine S., 2010, MNRAS, 401, 977
Kiman R. et al., 2021, AJ, 161, 277
King R. R., McCaughrean M. J., Homeier D., Allard F., Scholz R. D., Lodieu N., 2010, A&A, 510, A99
Kirkpatrick J. D. et al., 2011, ApJS, 197, 19
Kirkpatrick J. D. et al., 2021, ApJS, 253, 7
Kirkpatrick J. D. et al., 2024, ApJS, 271, 55
Lang D., 2014, AJ, 147, 108
Laureijs R. et al., 2011, preprint (arXiv:1110.3193)
Lépine S., Rich R. M., Shara M. M., 2007, ApJ, 669, 1235
LSST Science Collaboration, 2017, preprint (arXiv:1708.04058)
Lu Y., Angus R., Foreman-Mackey D., Hattori S., 2024, AJ, 167, 159
Luhman K. L., 2013, ApJ, 767, L1
Mace G. N. et al., 2013, ApJS, 205, 6
Mainzer A. et al., 2011, ApJ, 731, 53
Mann A. W. et al. 2019. ApJ, 871, 63
Marley M. S. et al., 2021, ApJ, 920, 85
Marocco F. et al., 2015, MNRAS, 449, 3651

Marocco F. et al., 2021, ApJS, 253, 8
Marocco F. et al., 2024, ApJ, 967, 147
McCaughrean M. J., Close L. M., Scholz R. D., Lenzen R., Biller B., Brandner W., Hartung M., Lodieu N., 2004, A&A, 413, 1029
McMahon R. G., Banerji M., Gonzalez E., Koposov S. E., Bejar V. J., Lodieu N., Rebolo R., VHS Collaboration, 2013, The Messenger, 154, 35
Murray D. N. et al., 2011, MNRAS, 414, 575
Nakajima T., Oppenheimer B. R., Kulkarni S. R., Golimowski D. A., Matthews K., Durrance S. T., 1995, Nature, 378, 463
Pinfield D. J. et al., 2012, MNRAS, 422, 1922
Rayner J. T., Toomey D. W., Onaka P. M., Denault A. J., Stahlberger W. E., Vacca W. D., Cushing M. C., Wang S., 2003, PASP, 115, 362
Rebolo R., Zapatero Osorio M. R., Martín E. L., 1995, Nature, 377, 129
Ricker G. R. et al., 2015, J. Astron. Telesc. Instrum. Syst., 1, 014003
Rothermich A. et al., 2024, AJ, 167, 253
Schlawin E. et al., 2014, in Ramsay S. K., McLean I. S., Takami H., eds, Proc. SPIE Conf. Ser. Vol. 9147, Ground-based and Airborne Instrumentation for Astronomy V. SPIE, Bellingham, p. 91472H
Scholz R. D., 2010, A&A, 510, L8
Scholz R. D., McCaughrean M. J., Lodieu N., Kuhlbrodt B., 2003, A&A, 398, L29
Skrutskie M. F. et al., 2006, AJ, 131, 1163
Soubiran C., Le Campion J.-F., Brouillet N., Chemin L., 2016, A&A, 591, A118
Sozzetti A., 2023, A&A, 670, L17
Spergel D. et al., 2015, preprint (arXiv:1503.03757)
Stassun K. G. et al., 2019, AJ, 158, 138
Thompson M. A. et al., 2013, PASP, 125, 809
Vernet J. et al., 2011, A&A, 536, A105
Wright E. L. et al., 2010, AJ, 140, 1868
Xuan J. W. et al., 2024, Nature, 634, 1070
Zhan H., 2011, Sci. Sin. Phys. Mech. Astron., 41, 1441
Zhang Z. H. et al., 2010, MNRAS, 404, 1817
Zhang Z. H. et al., 2017a, MNRAS, 464, 3040
Zhang Z. H. et al., 2018a, MNRAS, 479, 1383
Zhang Z. H. et al., 2018b, MNRAS, 480, 5447
Zhang Z. H. et al., 2024, MNRAS, 533, 1654
Zhang Z. H., Burgasser A. J., Gálvez-Ortiz M. C., Lodieu N., Zapatero Osorio M. R., Pinfield D. J., Allard F., 2019, MNRAS, 486, 1260
Zhang Z. H., Homeier D., Pinfield D. J., Lodieu N., Jones H. R. A., Allard F., Pavlenko Y. V., 2017b, MNRAS, 468, 261
Zhang Z., 2019, MNRAS, 489, 1423
Zhang Z., Liu M. C., Claytor Z. R., Best W. M. J., Dupuy T. J., Siverd R. J., 2021, ApJ, 916, L11

SUPPORTING INFORMATION

Supplementary data are available at *MNRAS* online.

onlinedata.zip

Please note: Oxford University Press is not responsible for the content or functionality of any supporting materials supplied by the authors. Any queries (other than missing material) should be directed to the corresponding author for the article.

This paper has been typeset from a TEX/LATEX file prepared by the author.